Dynamic Analysis Using the Portable Pavement Dynamic Cone Penetrometer

KOON MENG CHUA AND ROBERT L. LYTTON

The Pavement Dynamic Cone Penetrometer [PDCP] considered in this study is similar to the one used in South Africa. In this study, the PDCP was used in conjunction with an accelerometer mounted at the extreme top of the device. Acceleration, velocity, and displacement histories were obtained. The force history was obtained by matching the measured acceleration peaks with that calculated using a numerical model of PDCP. The Fast Fourier Transform (FFT) technique was used to transform the information recorded in real time to the frequency domain. Spectral analyses were performed, and soil-damping characteristics were obtained for two pavement sections. The study shows that it is possible to determine the hysteretic and the viscous damping ratios in situ using the method of dynamic analysis described here.

The Pavement Dynamic Cone Penetrometer [PDCP] considered in this study is similar to the one used in South Africa and studied by Kleyn et al. (*1*). Traditionally, methods were developed for using the PDCP to predict the California bearing ratio (CBR) value of soils (*1–3*) and, more recently, the elastic modulus as well (*4*).

In this study, the PDCP was used in conjunction with an accelerometer mounted at the extreme top position. The accelerometer was used to record the dynamic characteristics of the PDCP. Velocity and displacement histories were obtained from the accelerations measured. Dynamic analyses were then performed in the frequency domain, and soil-damping characteristics were obtained for two pavement sections.

PAVEMENT DYNAMIC CONE PENETROMETER

Testing using the PDCP basically involved dropping a sliding hammer of about 17.6 lbs over a height of 22.6 in. to drive a steel rod of about 6.8 lbs into the ground. The depth penetrated by the 60-degree cone of tempered steel located at the lower end of the steel rod as a result of a single blow from the hammer is an indication of the material properties of the medium. Figure 1 shows the configuration of the PDCP. The PDCP measurements are reported in terms of the penetration index which is the penetration depth resulting from one blow of the hammer.

The PDCP is commonly used to determine the CBR values of soil. The relationships of the penetration index to the CBR values were obtained by driving the PDCP into a medium with a known CBR value in the field or into a medium contained in a CBR mold or a container with controlled confining pressure when done in the laboratory (*1–3*). This author (*4*) recently developed a relationship of the penetration index to the elastic modulus. The model assumes the soil medium penetrated in one blow to be a horizontal disc; and upon penetration, the cone tip displaces the soil, a radial plastic shock wave propagates in the disc, and plastic deformation takes place. The approach was motivated by the penetration theory presented by Yankelevsky and Adin (*5*).

DYNAMIC ANALYSIS: BACKGROUND

In performing dynamic analyses, it is common for practicing engineers to model a structural system as consisting of masses connected by springs and dashpots. Soil-structure interfaces are also modeled in a similar fashion. Under an excitation force, the springs will respond according to the magnitude of that force instantaneously while the dashpots respond according to the rate with which that force is applied. This is especially evident in soils, in which the response usually lags the excitation input. This behavior is accounted for by damping. The various types of damping will be discussed in subsequent sections.

Waves excited in the soil are a complex form of oscillatory movement propagating through a medium. By complex, it is meant that two components can best describe the phenomenon: the real component and the imaginary component, which is usually associated with the time lag of the response. It is also well known that transient compound oscillations can be represented as sums of harmonic oscillations by means of Fourier series or integrals.

Fast Fourier Transform

Data recorded in real time can be transformed to the frequency domain using the Fourier transform. The

Texas Transportation Institute, Texas A&M University, 501 CE/TTI Building, College Station, Tex. 77843.

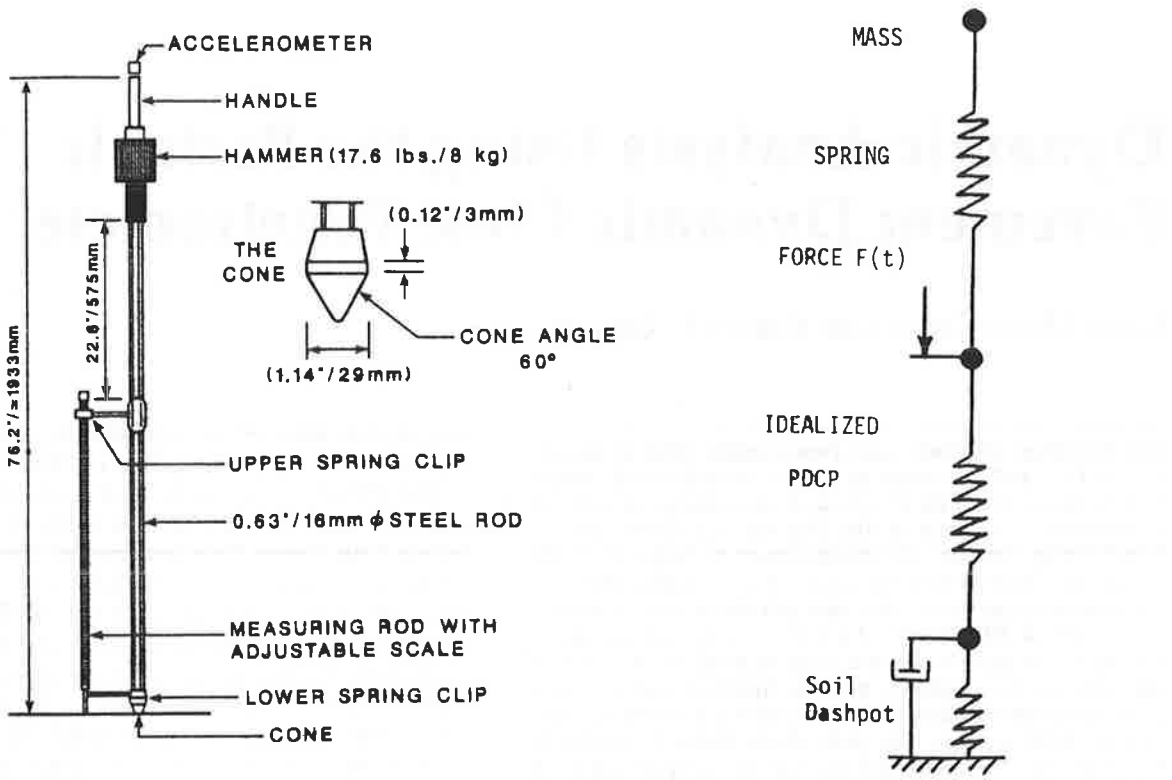

FIGURE 1 Pavement dynamic cone penetrometer.

Fourier transform of the function $x(t)$ is defined as

$$S_x(f) = \int_{-\infty}^{\infty} x(t) \exp(-2\pi i f t)\, dt \qquad (1)$$

where $S_x(f)$ = frequency domain representation of the function $x(t)$, and

$$i = \sqrt{(-1)}$$

If the function $x(t)$ is digitized, the above will be represented as a Discrete Fourier Transform [DFT] and is given by

$$S_x(m\Delta f) \doteq \Delta t \sum_{n=0}^{N-1} x(n\Delta t) \exp[-2i\pi(m\Delta f)(n\Delta t)] \qquad (2)$$

where

$S_x(m\Delta t)$ = digitized representation of the Fourier transform,
N = number of digitized points,
$t = 0, +/-1, +/-2 \ldots$, and
Δf = frequency interval between digitized points.

The time and frequency intervals are related by

$$\Delta f = 1/(N\Delta t) \qquad (3)$$

The Fast Fourier Transform [FFT] (*6*) technique is simply an algorithm that can compute the DFT much more rapidly than other available algorithms.

Damping

A dynamic system undergoing free vibration will eventually come to a halt. The system is said to have undergone damping, in which energy is being dissipated from the system. Damping is usually expressed as a damping ratio, which is the proportion of damping constant to the critical damping constant. A system with a damping ratio greater than 1.0 does not oscillate and is said to be overdamped. Conversely, an underdamped system will oscillate.

Damping is typically classified as structural or internal damping, viscous damping, dry damping, and negative damping. Structural damping is due to internal friction within the material or at connections between the elements of a dynamic system. This is usually explained by the hereditary theory, which attributes the loss of energy to the elastic delay by which the deformation lags behind the applied force. The latter is more commonly referred to as hysteretic damping and is thought to be independent of frequency. Viscous damping occurs, for example, in lubricated sliding surfaces, dashpots, and shock absorbers and is velocity- and frequency-dependent. Dry damping or Coulomb damping results from the motion of a body on a dry surface. The last and probably the least known is negative damping, which results when the nature of damp-

ing is such that instead of dissipating energy from the system, energy is added to it (*7*, pp. 123–125). However, linear viscous damping still occupies the major place in dynamic analysis, and as such, it is common to use equivalent viscous damping ratios (*8*, *9*) to represent the effects of hysteretic damping.

Complex Formulation of Damping

Consider the equations of motion of a structural system expressed in the matrix form. In the time domain, the equations of motion can be expressed as

$$[K]\{r\} + [C]\{\dot{r}\} + [M]\{\ddot{r}\} = \{R\} \tag{4}$$

where

$[K]$ = stiffness matrix,
$[M]$ = mass matrix,
$[C]$ = damping matrix,
$\{R\}$ = load matrix, and
$\{r\}$, $\{\dot{r}\}$ and $\{\ddot{r}\}$ = the displacement, the velocity, and the acceleration matrix, respectively.

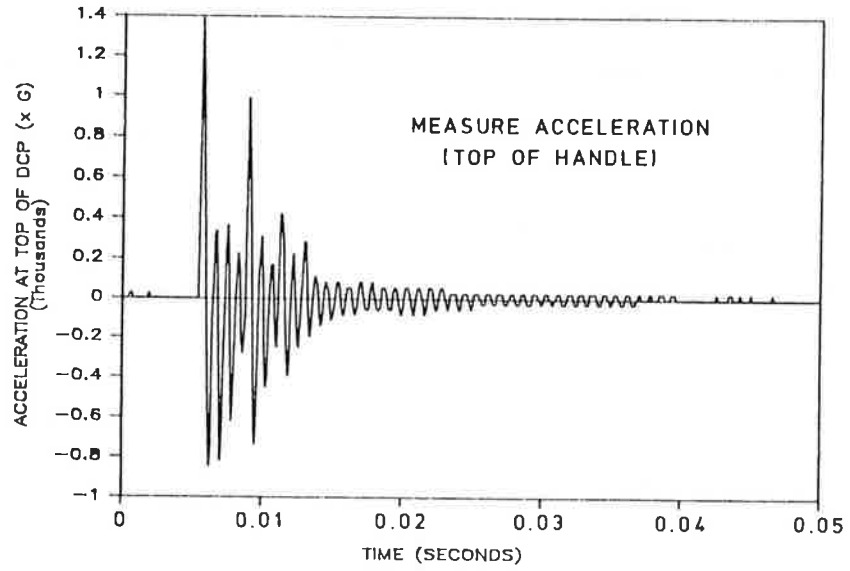

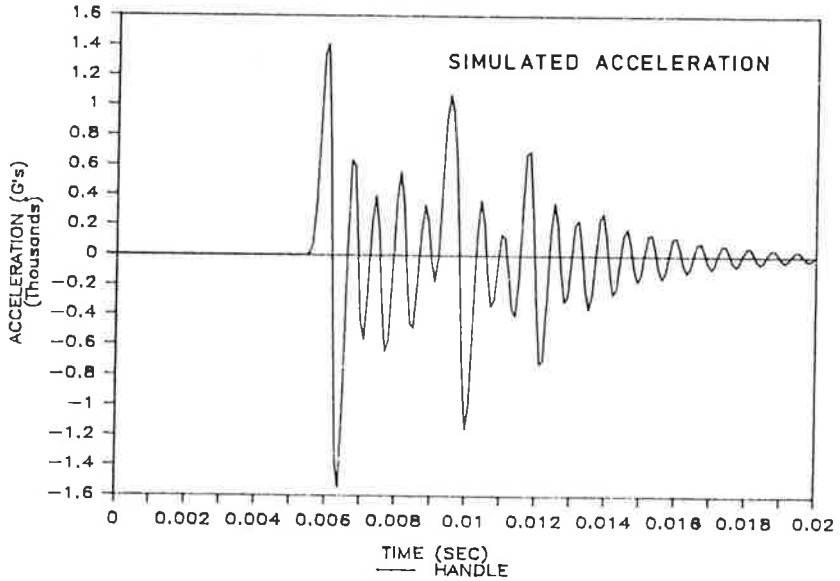

FIGURE 2 Comparing measured and simulated acceleration of the PDCP.

Transforming the above sets of equations into the frequency domain gives

$$([K] + i\omega[C] - \omega^2[M])\{U(\omega)\} = \{S(\omega)\} \quad (5)$$

where

ω = angular velocity (radians/sec),
$\{U(\omega)\}$, $\{S(\omega)\}$ = the Fourier transforms of the $\{r(t)\}$ and $\{R\}$, respectively.

The complex stiffness matrix $[K^*]$ is related to the stiffness and the damping by

$$[K^*] = [K] + i\omega[C_V] \quad (6)$$

where the subscript V refers to viscous damping.

In a single-degree-of-freedom system with both hysteretic and viscous damping, it has been shown (*10*) that the complex stiffness can be expressed by

$$k^* = k(1 + 2i\beta_H + 2i\beta_V) \quad (7)$$

and, if only hysteretic damping is present,

$$k^* = k(1 + 2i\beta_H) \quad (8)$$

where

β_H = the hysteretic damping ratio, and
β_V = the viscous damping ratio.

The above are two of the many models that have been proposed to describe damping. These will be compared

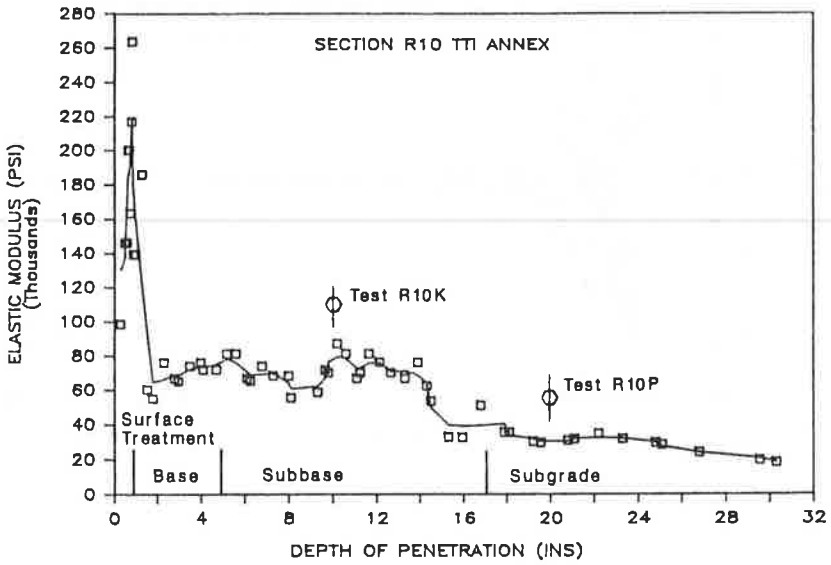

FIGURE 3 Layer characteristics and elastic modulus of section R10.

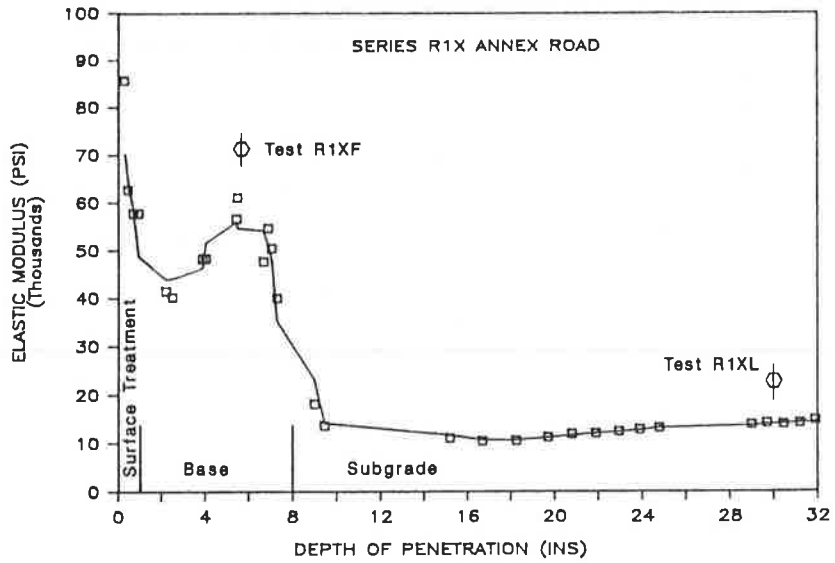

FIGURE 4 Layer characteristics and elastic modulus of section R1X.

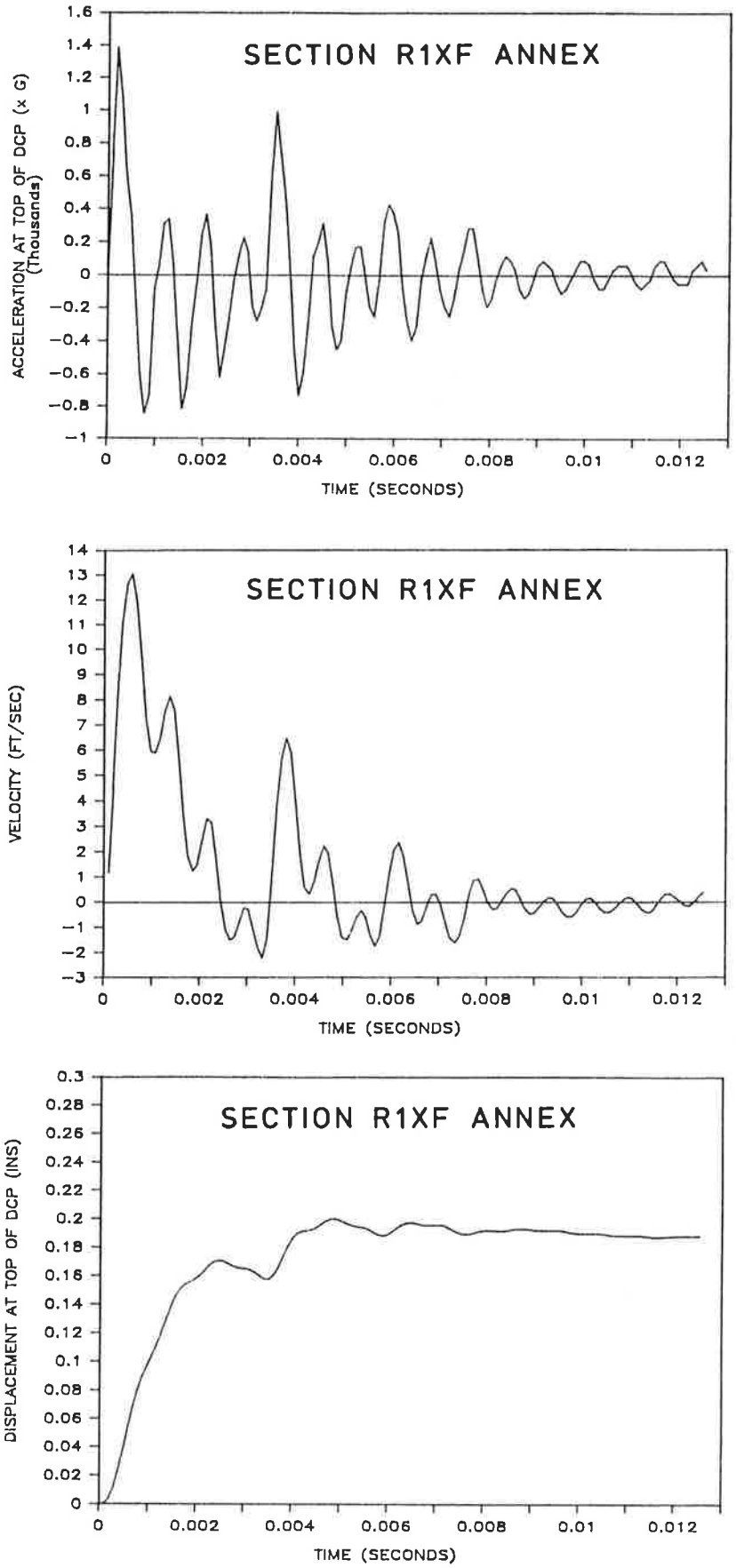

FIGURE 5 Typical acceleration, velocity and displacement histories of the PDCP in medium stiff granular base course material.

with field-measured ratios that will be presented in subsequent sections.

METHOD OF DYNAMIC TESTING USING THE PDCP

An accelerometer was screw-mounted onto the top of the handle of the PDCP (Figure 1). The accelerometer was rated for a shock of up to 100,000 G (where G is the gravitational acceleration) and up to 180 kHz. A 0.05-sec history containing 512 digitized points was recorded for each drop of the PDCP. The recording is triggered by the impact, and a certain amount of pre-impact history is also recorded.

The response considered here, which is the displacement history was obtained by double-integrating the acceleration history. The amplitudes of these impulses were obtained by matching the calculated acceleration peaks with the measured acceleration peaks for all the test cases considered. The calculated acceleration peaks were obtained using a computer program that models the dynamic response of the PDCP under impact load. The program is described below.

Numerical Modeling

To anticipate the dynamic response of the PDCP, a simple computer program was written to model the PDCP as a three-degree-of-freedom structure supported at the cone

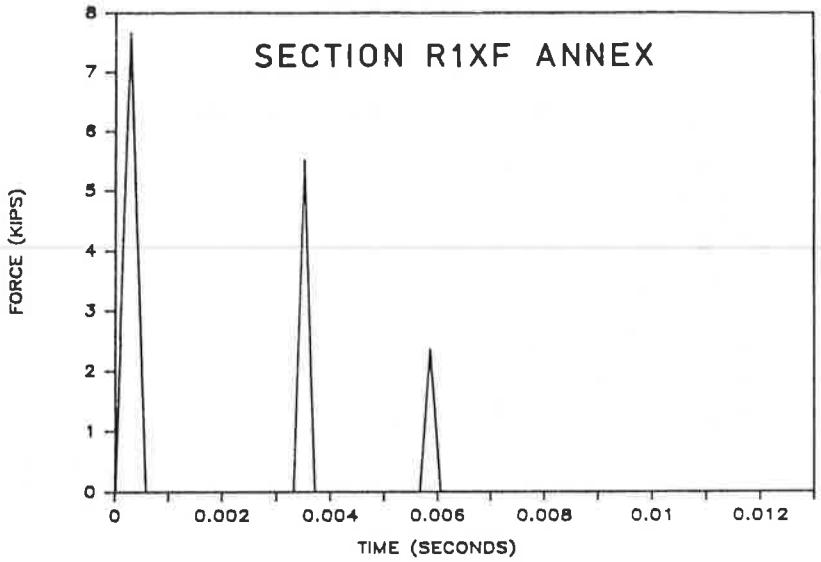

FIGURE 6 Typical calculated force history of the PDCP in granular base course material.

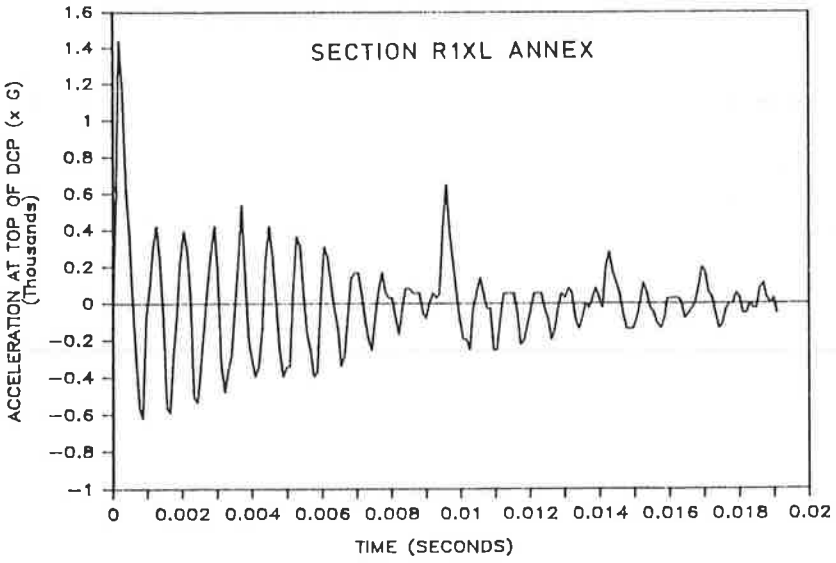

FIGURE 7 Typical acceleration history of the PDCP in silty clay subgrade.

tip by an external spring and a dashpot (Figure 1). It is assumed that the damping within the PDCP is negligible and that the system is damped mainly through the cone tip, which is the only part of the PDCP in contact with the soil.

The force history of the sliding hammer onto the middle of the PDCP consisted of impulses simulated as triangularly shaped force input over a short period of time. The several time periods during which the sliding hammer was in contact with the rod were obtained from the accelerometer reading. The amplitudes of the impulses were obtained by matching the calculated initial acceleration of the point in which the accelerometer was mounted (at the top of the handle) with that measured. The algorithm (*11*, pp. 387–402) performs the step-by-step integration of the equations of motion represented by equation 4 for a multidegree-of-freedom system using the linear acceleration method with the Wilson-θ modification. The latter serves to assure the numerical stability of the solution process regardless of the magnitude selected for the time step.

Figure 2 compares the calculated and the measured acceleration history of one of the tests. The period of the impulse (in this case, the first impulse peaked at 7.75 kips and occurred over 0.0006 sec) was obtained from the first measured acceleration peak. The positive acceleration refers to the downward direction.

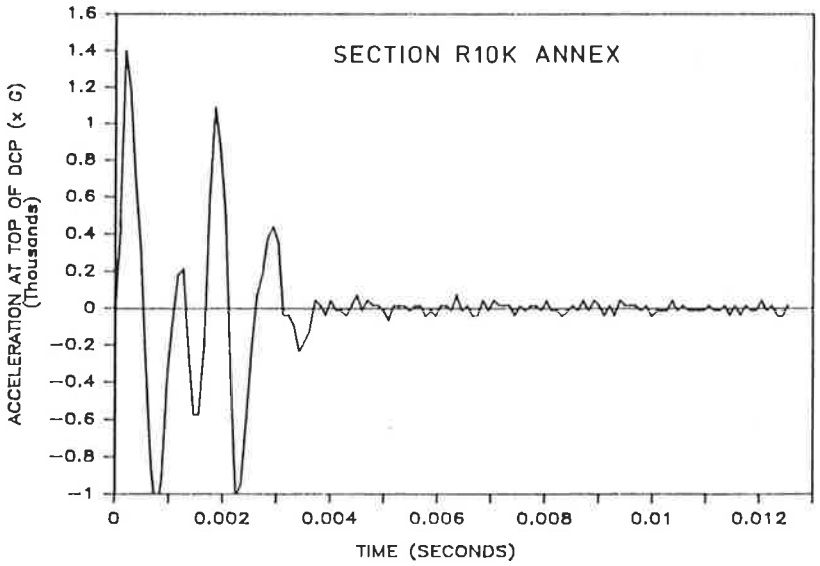

FIGURE 8 Typical acceleration history of the PDCP in stiff granular base course material.

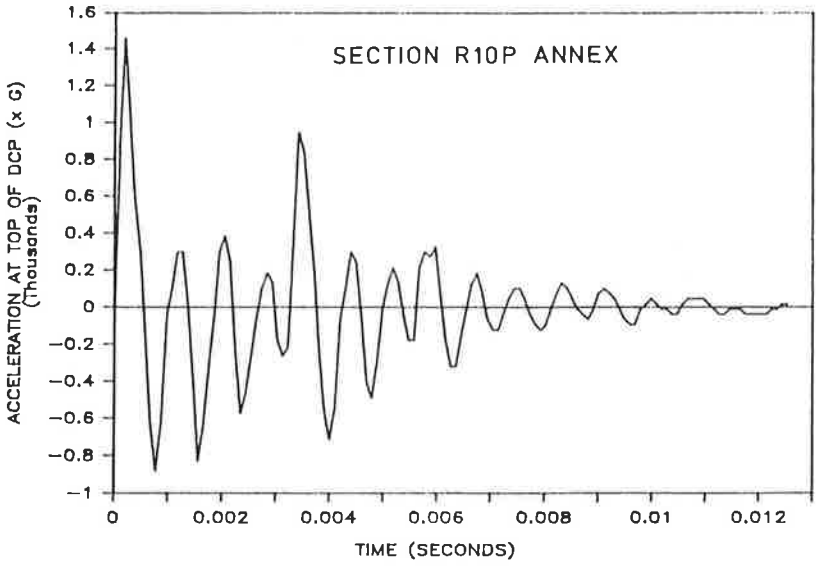

FIGURE 9 Typical acceleration history of the PDCP in sand-gravel subgrade.

Field Testing

Two pavement sections were used in this study. The section configurations and the interpreted elastic modulus profiles obtained using the method described in Chua (*4*) are shown in Figures 3 and 4. Both sections were located at the Texas Transportation Institute Test Annex. The first section, marked R10 (Figure 3), consisted of a 1-in.-thick surface treatment course, over a 4-in. base course and a 12-in. second layer of base of the same crushed stone materials. The subgrade is sand-gravel. Section R1X (Figure 4) is in an access road (near the test section facility) and is a surface-treated pavement with a 7-in. base course and a silty clay subgrade.

Figure 5 shows the acceleration, velocity, and displacement history of a test performed in a granular base course material (test R1XF) in Section R1X. The force history obtained using the numerical model described earlier is shown in Figure 6. Three other typical acceleration histories obtained are shown in Figures 7 through 9. The materials represented by these four tests are a stiff base consisting of crushed stones (test R10K), a loosely

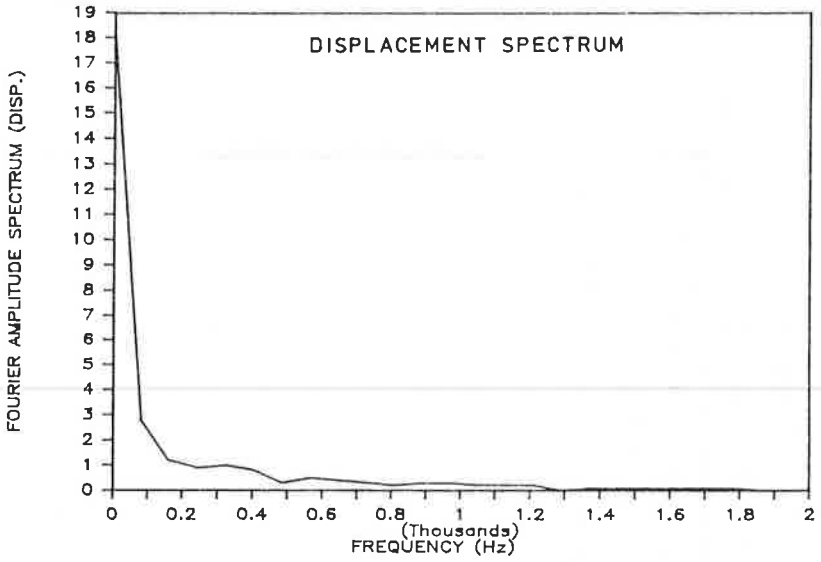

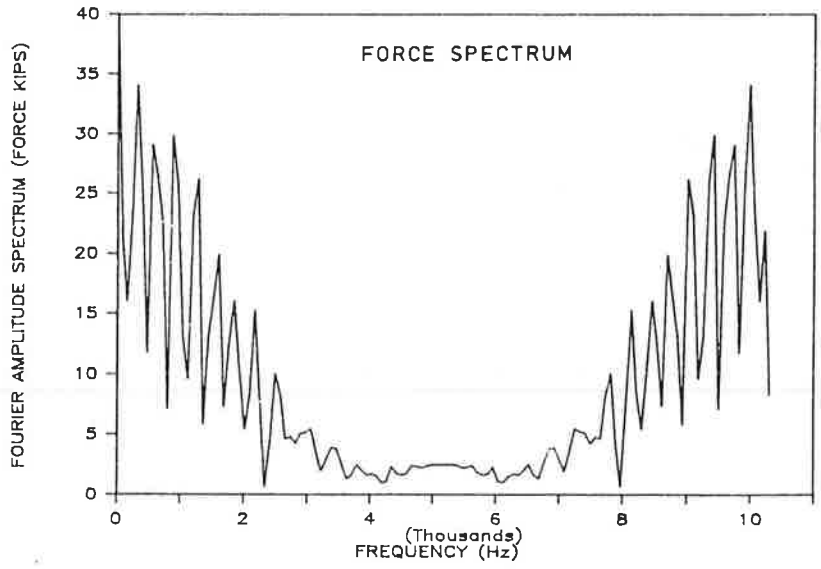

FIGURE 10 Typical PDCP displacement and force spectra.

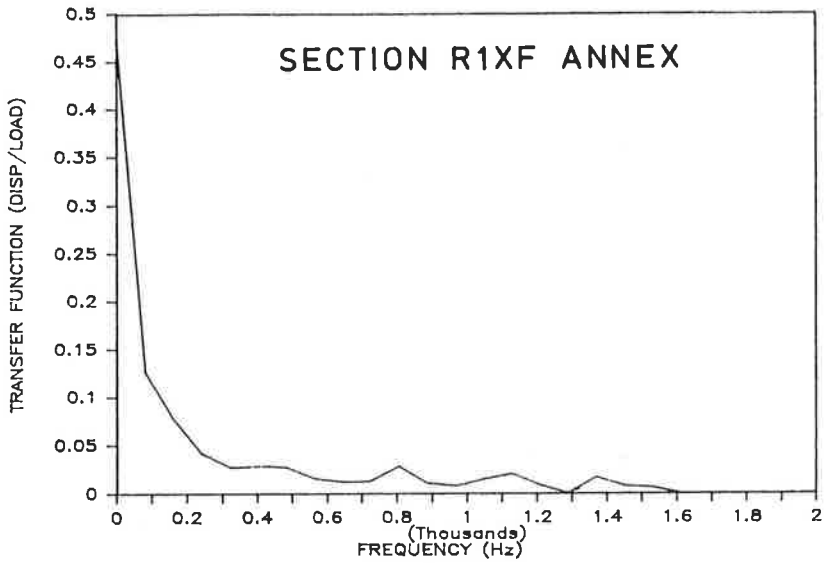

FIGURE 11 Typical transfer function in the frequency domain.

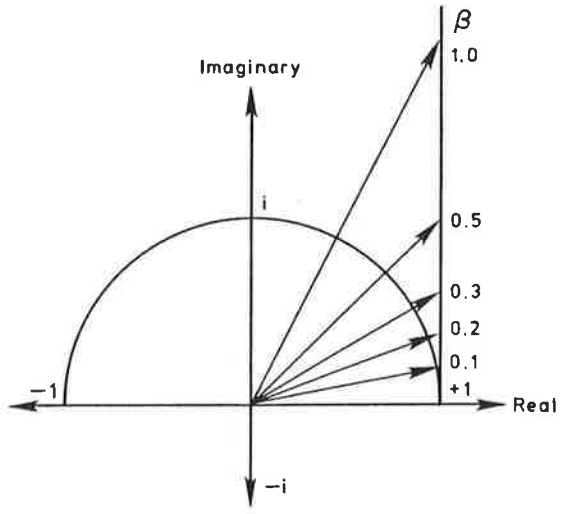

FIGURE 12 Complex damping ratio.

bounded base (test R1XF), sand-gravel subgrade material (test R10P), and a silty clay subgrade (test S1XL). The test identifications are given in parentheses and the respective depths at which the soil was tested are also shown in Figures 3 and 4.

Digital Signal Analysis

Continuing to use test R1XF as an example, the displacement history and the force history that were obtained were transformed into the frequency domain using FFT, and the resulting spectra are shown in Figure 10. In this example, only a period of 0.0124 sec (composed of 128 digitized points), which includes most of the predominant signals, was used because signals recorded before the impact and some times beyond this time period consist mainly of noise, and including them will introduce errors into the spectral analysis. The transfer function, which consists of each component of the displacement spectrum divided by the force spectrum at the corresponding frequency, is shown in Figure 11.

The damping ratio β, in accordance with equation 8 can be obtained from the two components of the complex transfer function by halving the tangent of the lag angle between the real and the imaginary component as shown in Figure 12. The damping ratios for the frequency spectrum obtained for the pavement materials in the two sections are shown in Figures 13 and 14.

DISCUSSION OF RESULTS

Dynamic Behavior of the PDCP

From the acceleration histories shown earlier, it can be seen that the sliding hammer struck the rod several times. In the case of the loose base course (test R1XF, elastic modulus of 60,000 psi), three blows were recorded. The time interval between impact can be seen to vary for different soil types. It can also be seen that the peak is at about 1,400 G for all cases, which implies that the first and most critical force impulse is very similar for all cases. This similarity can be expected because the impact, between steel and steel, occurs over such a short period of time that the whole system is not set in motion yet. This makes the determination of the force history (from the numerical model) a much easier one.

The velocity (referring to Figure 5), as expected, approaches zero with time. The measured displacement for all cases approaches a nonzero asymptote. This will differ from the prediction made using the simple numerical model because the latter assumed a linear elastic spring, whereas in the real case, plastic deformation occurs. For

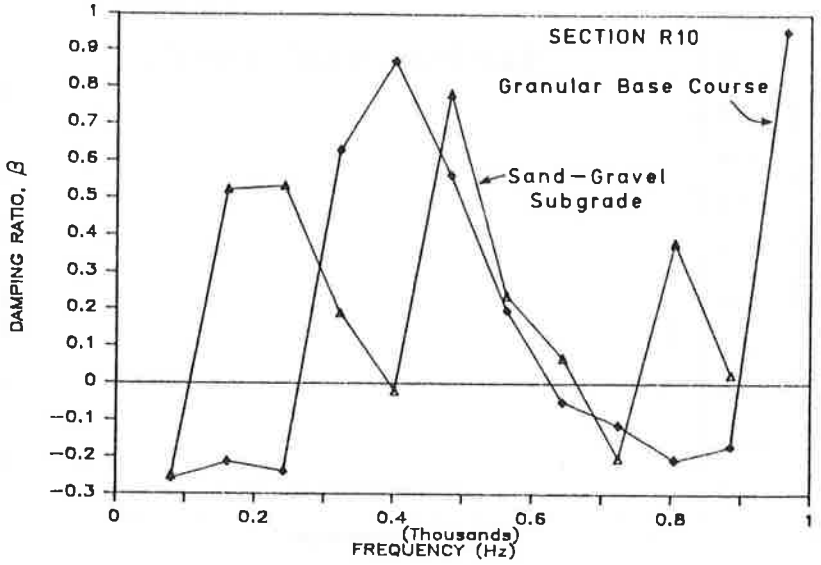

FIGURE 13 Damping ratios determined from spectral analysis for Section R1X.

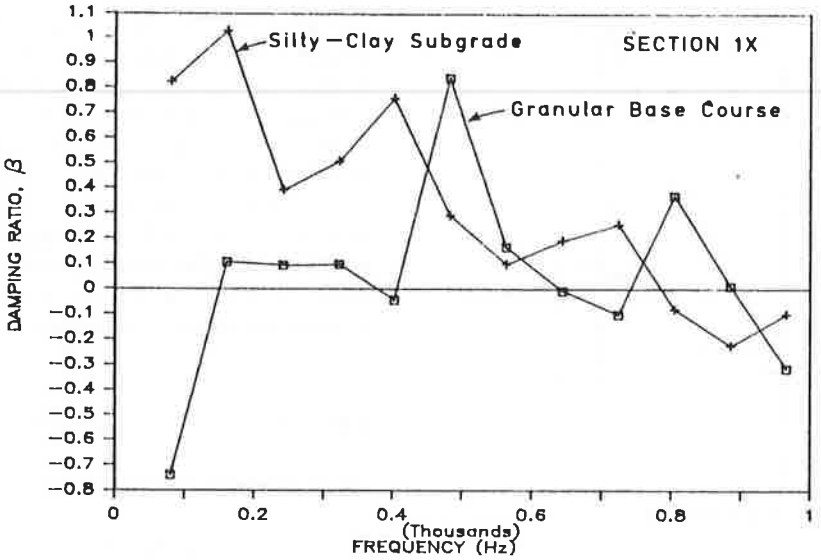

FIGURE 14 Hysteretic and viscous damping ratios.

the same reason, the numerical simulation will show the displacement approaching zero with time.

Damping Ratios

The predominant frequency band, identified from the transfer function spectrum for all the tests performed, was found to be from 0 to 1 kHz (Figure 11). This means that data manipulation performed within this range will be fairly accurate.

Referring to Figures 13 and 15 and assuming that all the damping in the system is due to the hysteretic damping from the soil, the damping ratios obtained suggest that negative damping does exist. While it is not possible at this time to account for this phenomenon (negative damping), it appears that the mean of the damping ratios over the 1 kHz range is still in the positive range. The mean damping ratios for the two base course materials tested were found to be 0.04 and 0.16. The damping ratio for the sand-gravel and the silty clay subgrade was found to be 0.33 and 0.21 respectively. These damping ratios were averaged over the 1 kHz range and assumed to be independent of frequency, as is described by equation 8. These averaged damping ratios are in the range expected of materials such as these (*12*). However, their obvious dependence on frequency suggests further inquiry.

If equation 7 is used, that is, the viscous damping ratio is linearly dependent on the angular velocity or the frequency, then by fitting a line through the data shown in

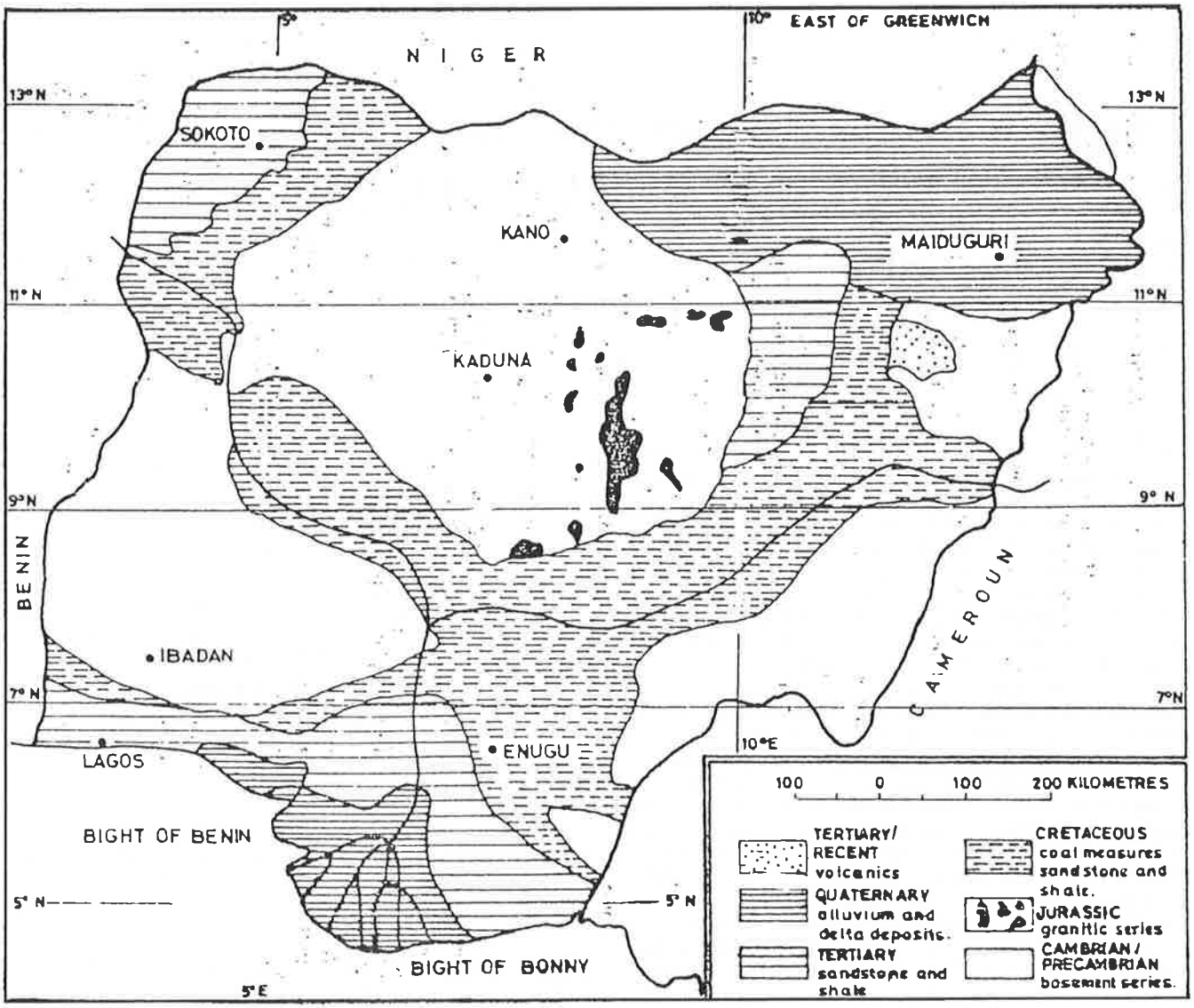

FIGURE 1 Geological map of Nigeria.

tically pitted or vesicular appearance of massive laterites, although termites have also been credited with causing the pitting.

The leaching in solution of colloidal silica and alkalis leaves a residue, which is relatively rich in hydrated oxides of aluminum, iron, and titanium. This iron enrichment produces the red color typically associated with laterite soils. There are, of course, some soils that do not owe their coloration to laterization. Also, the bonding effect of the iron oxides often produces a soil matrix with low compressibility, high permeability, and high angle of shearing resistance for these residual soils (*11*, *12*).

In situ laterites often have a cap rock of cuirasse or iron stone below the softer products of weathering, due to the increasing degree of saturation of the percolating water and the consequent reduction in the rate of solution as it travels downward. This process of weathering takes place everywhere in the country except in the low lands of the extreme southern part where the average annual rainfall is more than 200 cm (80 in.), where mangrove swamp vegetation occurs, and along the flood plains of the many rivers running north-south from the highlands.

In the far northern areas above latitude 11 degrees north, where annual rainfall is generally less than 75 cm and savannah vegetation predominates, the existence of basalts and other tertiary volcanic rocks has led to the formation of high activity clays (vertisols) characterized by extreme shrinkage and swelling characteristics. These are the local black cotton soils and clay shales of northern Nigeria, as found in parts of Bauchi, Borno, Gongola, Kano, and Sokoto states. These soils have been discussed in the literature (*8*, *10*, *13–16*).

CLASSIFICATION

Residual soils are ill defined and of variable origin, which makes their classification difficult. Soil samples may in-